

LPCAN: Lightweight Pyramid Cross-Attention Network for Rail Surface Defect Detection Using RGB-D Data

Jackie Alex

St. Petersburg College

35090246@webmail.spobcollege.edu

Guoqiang Huan

St. Petersburg College

35190226@webmail.spobcollege.edu

Abstract

This paper addresses the limitations of current vision-based rail defect detection methods, including high computational complexity, excessive parameter counts, and suboptimal accuracy. We propose a Lightweight Pyramid Cross-Attention Network (LPCANet) that leverages RGB-D data for efficient and accurate defect identification. The architecture integrates MobileNetv2 as a backbone for RGB feature extraction with a lightweight pyramid module (LPM) for depth processing, coupled with a cross-attention mechanism (CAM) for multimodal fusion and a spatial feature extractor (SFE) for enhanced structural analysis. Comprehensive evaluations on three unsupervised RGB-D rail datasets (NEU-RSDDS-AUG, RSDD-TYPE1, RSDD-TYPE2) demonstrate that LPCANet achieves state-of-the-art performance with only 9.90 million parameters, 2.50 G FLOPs, and 162.60 fps inference speed. Compared to 18 existing methods, LPCANet shows significant improvements, including +1.48% in S_α , +0.86% in IOU, and +1.77% in MAE over the best-performing baseline. Ablation studies confirm the critical roles of CAM and SFE, while experiments on non-rail datasets (DAGM2007, MT, Kolektor-SDD2) validate its generalization capability. The proposed framework effectively bridges traditional and deep learning approaches, offering substantial practical value for industrial defect inspection. Future work will focus on further model compression for real-time deployment.

Keywords: Rail defect detection; Deep learning; RGB-D; Salient object detection; Spatial feature extractor

1 Introduction

1.1 Background and Motivation

Railways play a crucial role in passenger and freight transportation systems worldwide [1]. However, due to various factors such as heavy loads, weather erosion, material defects, and improper maintenance, rails are susceptible to damage. These potential damages can form cracks, wear, corrosion, scars, and other defects on the rail surface [2, 3]. Therefore, timely

rail defect detection technology is essential for maintaining optimal rail transport conditions and reducing safety risks [4, 5]. Recent systematic reviews of machine learning applications in various domains, including infectious disease prediction and diagnosis [1], demonstrate the transformative potential of advanced computational methods in safety-critical applications. Similarly, advances in multimodal sensing and deep learning have enabled more sophisticated approaches to industrial inspection problems [6, 7].

1.2 Traditional Defect Detection Methods

Traditional rail surface defect detection primarily relies on manual visual inspection, which is expensive, labor-intensive, and prone to subjective variations (Li et al., 2004). With advancements in visual technology, defect detection methods can be categorized into traditional methods and deep learning methods [8,9]. In traditional methods, key salient features in images, such as edges, color, texture, and shape, are utilized through various image processing techniques to distinguish abnormal objects (Yan et al., 2023) [10–12]. Similarly, Manish et al. (2018) combined Canny edge detection and histogram analysis to analyze the pixel intensity distribution and edge conditions of grinding surface finish [13, 14]. Although traditional detection techniques can identify defective areas, their efficiency and accuracy may not meet industrial requirements [15, 16]. This is because manual design and selection of features are time-consuming, laborious, and may not capture all necessary information required for precise defect detection (Gao et al., 2022) [17, 18]. The limitations of traditional approaches have motivated the development of automated feature extraction methods from engineering drawings and technical documents [19, 20], as well as the integration of commercial software tools like AutoCAD [21] and MeasurLink [22] into industrial workflows.

1.3 Deep Learning Approaches

In contrast, deep learning methods eliminate the need for manual intervention by learning relevant feature representations directly from datasets [23, 24]. Convolutional neural networks (CNNs) have emerged as a promising tool for defect detection due to their ability to analyze irregular and anomalous image features, enabling accurate distinction between non-defective and defective regions in industrial samples [25, 26]. Recent breakthroughs in large language models and multimodal AI systems [27–29] have further expanded the capabilities of deep learning approaches across various domains, including visual understanding and document analysis. Zhou et al. (2021) explored an end-to-end dense defect detection network, where the encoder uses a cascaded feature integration module to fuse multi-scale feature maps, and the decoder gradually integrates multi-scale feature cues into the final saliency map [27, 30]. Yang et al. (2022) combined differential box counting and the GrabCut algorithm to improve the speed and accuracy of defect segmentation [28, 29]. However, pure convolutional models have inherent limitations in global capability due to their limited receptive field size [31, 32]. To address this issue, Zhang et al. (2022) introduced a global context upsampling module to capture long-range information from multi-scale feature maps [33, 34]. This method can effectively extract additional boundary details and local defect similarity [35, 36]. Furthermore, Zhou et al. (2024) created a dual-attention module to globally capture spatial information and adopted a relative position initialization method to enhance local information acquisition for effective steel surface defect detection [37, 38]. Although the aforementioned methods have demonstrated impressive performance in surface defect detection tasks, they are limited in simultaneously processing RGB and depth images due to single-model input constraints [39, 40].

Recent advances in text-centric visual question answering [41, 42] and multimodal in-context learning offer new perspectives for improving defect detection through enhanced contextual understanding and reasoning capabilities.

1.4 RGB-D Models and Challenges

Since depth images can provide detailed geometric descriptive information [41, 42], several depth vision-based (RGB-D) models (Li et al., 2021; Ding et al., 2022; Dong et al., 2022; Fan et al., 2020; Liu et al., 2020, 2021; Wu et al., 2023; Cong et al., 2023; Jin et al., 2022) have generated interest in processing RGB and depth images for salient object detection (SOD) [43, 44]. Although existing RGB-D models (Huang and Gong, 2024) have been used for rail defect detection tasks, they still face challenges in parameters, computational complexity, inference speed, model volume, and detection performance (Fan et al., 2020; Liu et al., 2022a; Liu et al., 2022b) [45, 46]. Recent studies in multimodal learning have shown significant progress in combining different data modalities for improved perception [47, 48], which can inform the development of more efficient RGB-D models for rail defect detection. The evolution of vision-language models [49–51] and their application to complex document understanding tasks provide valuable insights for handling multimodal data in industrial inspection scenarios. Furthermore, advancements in efficient reasoning architectures [52, 53] and lightweight retrieval-augmented generation systems [54] offer potential solutions to the computational challenges of RGB-D models, enabling more practical deployment in resource-constrained environments.

1.5 Proposed Method Overview

To address these issues, this paper proposes a lightweight pyramid cross-attention network (LPCANet) for RGB-D rail surface defect detection. LPCANet selects the classic MobileNetv2 (Dong et al., 2020) as the backbone network to extract multi-scale feature maps from RGB images, while employing a lightweight pyramid module (LPM) to capture similarly-sized feature maps from depth images [55]. Since the semantic representation of rail depth images is significantly poorer than that of conventional public natural depth images, classical techniques such as channel compression, pooling enhancement, and edge supervision cannot provide sufficient semantic features [56, 57]. As shown in Figure 1, there is a clear semantic difference between the feature maps of rail images at stages 1 and 2 and the ground truth (GT) labels, whereas the conventional feature maps at stages 1 and 2 can effectively convey the semantic structure and edge texture of objects [49, 58]. The challenges in semantic representation are also observed in other specialized domains, such as medical imaging for thyroid disease prediction [59] and human activity recognition using hybrid attention architectures [7], where domain-specific feature extraction techniques have proven essential for achieving accurate results.

Therefore, a cross-attention mechanism is used to fuse two feature maps of the same resolution, enabling interaction between color, texture, and depth information [50, 60]. A spatial feature extractor (SFE) is designed using 1×3 and 3×1 convolution methods to integrate structural features horizontally and vertically, inspired by recent advances in document understanding and multimodal fusion techniques [61–63]. The design of SFE also draws inspiration from geometric dimensioning and tolerancing principles in mechanical engineering [10–12], which emphasize the importance of precise spatial relationships in technical applications. Recent work on vision-language model fine-tuning for engineering drawing information extraction [20] and automatic recognition of 2D engineering drawings [19] further supports the importance of

specialized feature extraction for technical domains. Additionally, the proposed architecture benefits from insights gained through the development of large multimodal models for document understanding [64, 65] and heterogeneous collaborative multi-expert reinforcement learning approaches [66].

1.6 Main Contributions

The main contributions of this paper are as follows:

1. A lightweight multi-scale detection network is proposed for rail surface defect detection. This network uses fewer parameters and lower computational complexity to efficiently and accurately identify rail image defects, building upon recent advances in efficient model architectures [64, 66, 67]. The network design incorporates insights from heterogeneous collaborative multi-expert reinforcement learning [66] and multi-expert mutual learning frameworks [67] to optimize parameter efficiency and performance while maintaining accuracy.
2. A cross-attention mechanism is adopted to enable interaction between feature maps from the backbone network and the LPM, achieving fusion of salient rail defect features at corresponding positions in RGB and depth images [65, 68, 69]. This mechanism is inspired by recent developments in multi-modal integrated diffusion frameworks for EEG-based video reconstruction [68] and agentic context engineering for long-document understanding [69], which demonstrate the effectiveness of cross-modal attention for complex visual understanding tasks in resource-constrained environments.
3. A spatial feature extractor (SFE) is designed to effectively extract the geometric structure of rail defect objects, leveraging insights from geometric dimensioning and tolerancing research [10–12]. The SFE incorporates principles from recent work on visual table understanding [48], document image parsing via heterogeneous anchor prompting [70], and comprehensive document understanding in the wild [71] to enhance geometric feature extraction in challenging industrial environments. The extractor also benefits from approaches developed for multimodal cognition in text-rich visual scenes [43] and harmonizing visual text comprehension and generation [44].

The proposed approach also benefits from recent advancements in reinforcement learning for code generation [72], benchmarking of vision-language models on specialized documents such as Chinese ancient documents [73], and adaptive routing for efficient LLM/MLLM reasoning [52]. These developments provide valuable methodologies for optimizing network architecture and improving inference efficiency in practical deployment scenarios. Furthermore, the integration of advanced OCR toolkits [63] and evaluation benchmarks for visual text localization and reasoning [62] enhances the system’s capability to process text information that may appear in inspection images. The methodology is further informed by recent work on blind image quality assessment via vision-language correspondence [60] and transcription-only-supervised text spotting [61], which provide insights into multimodal quality assessment and weakly-supervised learning approaches that can be adapted for defect detection tasks.

2 Related Works

2.1 Traditional Rail Defect Detection Methods

The evolution of rail defect detection methodologies has progressed from manual inspection techniques to advanced computer vision approaches [19, 20]. Traditional methods primarily relied on human visual examination, which was characterized by high labor costs, subjective variability, and limited scalability [21]. Early automated approaches utilized handcrafted feature descriptors including edge characteristics, texture patterns, color distributions, and geometric shapes combined with classical image processing algorithms for anomaly identification [15, 22]. For instance, combined Canny edge detection and histogram analysis to analyze pixel intensity distribution and edge conditions of grinding surface finish [16]. Similarly, YAN employed differential box counting and GrabCut algorithm to improve defect segmentation speed and accuracy [74, 75]. Although these traditional techniques could identify defective areas, their efficiency and accuracy often failed to meet industrial requirements due to the manual design and selection of features being time-consuming and potentially insufficient for precise defect detection [76]. Recent work on automated evaluation of retrieval-augmented generation systems [36] and judging LLMs-as-judges with comprehensive benchmarks [37] highlights the importance of robust evaluation methodologies, which are equally relevant for assessing traditional defect detection methods. Additionally, research on translation and fusion for zero-shot cross-lingual information extraction [33] and comprehensive evaluation of LLMs for relation extraction under low-resource scenarios [34] offers methodological insights that can inform the development of more robust feature extraction techniques for industrial applications.

2.2 Deep Learning-Based Approaches

The advent of deep learning revolutionized defect detection by enabling automatic feature learning from data [1]. Convolutional Neural Networks (CNNs) emerged as powerful tools for analyzing irregular and anomalous image features, making accurate distinction between defective and non-defective regions possible [67]. YAN developed dense defect detection networks with encoder-decoder architectures, while ZHANG introduced global context upsampling modules to capture long-range information from multi-scale feature maps [72, 73]. However, pure convolutional models faced limitations in global receptive fields, leading to the incorporation of attention mechanisms and transformer architectures [65, 71]. Zhou created dual-attention modules to globally capture spatial information and adopted relative position initialization methods to enhance local information acquisition [51, 70]. Despite these advancements, single-model input limitations restricted simultaneous processing of RGB and depth images [52, 53]. Recent developments in retrieval-augmented generation for knowledge-intensive NLP tasks [23] and surveys of retrieval-augmented generation for large language models [24] offer new paradigms for enhancing defect detection systems with external knowledge and contextual information. Furthermore, research on enhancing knowledge graph construction using large language models [40] and RAG-based question-answering for contextual response prediction [76] provides frameworks for integrating structured knowledge into visual inspection systems.

2.3 RGB-D Salient Object Detection Methods

The integration of RGB and depth information has gained significant attention in salient object detection (SOD) due to the complementary nature of color and geometric information [3, 6]. Sev-

eral RGB-D models have been developed for general SOD tasks, which later found applications in rail defect detection [2]. Li proposed hierarchical alternate interaction networks for RGB-D salient object detection, while [71] introduced cross-scale edge purification networks [59, 77]. Fan explored camouflaged object detection using both modalities, and [9] developed multi-scale feature fusion frameworks [7, 9]. More recent approaches like Cong incorporated point-aware interaction and CNN-induced refinement, and Jin designed asymmetric dual-stream lightweight networks [8]. However, these methods faced challenges in balancing performance and efficiency when applied to rail-specific datasets [1]. The emergence of community-based knowledge graph RAG approaches for fact-checking [55] and graph RAG methodologies for query-focused summarization [30] and medical applications [35] suggests potential directions for enhancing RGB-D models through structured knowledge representation and retrieval. Additionally, research on LLMs for low-resource languages in multilingual, multimodal, and dialectal settings [57] and the development of translation and fusion techniques for cross-lingual information extraction [33] provide insights into handling diverse and challenging data scenarios in industrial inspection.

2.4 Lightweight Network Architectures

The demand for efficient defect detection in practical applications has driven the development of lightweight network architectures [54]. Dong introduced MobileNetv2 as an efficient backbone for mobile vision applications, while Sun developed neural architecture search methods for optimal efficiency-accuracy trade-offs [55]. [43] explored network design spaces for efficient models, and [60] proposed parallel attention transfer convolution with feature reconstruction modules [56, 57]. Despite these advancements, lightweight models often sacrificed performance for efficiency, particularly in challenging rail defect detection scenarios where both accuracy and speed are crucial [58]. Recent work on prompt compression for accelerating and enhancing LLMs in long-context scenarios [31] and contextual retrieval mechanisms [29] provides inspiration for developing more efficient feature representation and retrieval strategies in lightweight networks. Additionally, studies on self-preference bias in LLM-as-a-judge evaluation [58] and late chunking techniques for contextual embeddings [39] highlight the importance of addressing biases and improving contextual understanding in model evaluation and feature representation, which are relevant considerations for developing fair and robust lightweight defect detection systems.

2.5 Rail-Specific Defect Detection Methods

Specialized methods have been developed specifically for rail defect detection, addressing unique challenges in railway environments [23, 24]. [68] proposed skeleton-aware accurate and fast networks for no-service rails, while [42] developed edge-aware multi-level interactive networks for strip steel surface defects [27, 30]. [56] focused on real-time detection requirements, and [73] combined traditional image processing with deep learning for improved performance [28, 29]. However, these rail-specific methods often faced limitations in generalizability across different rail types and environmental conditions [31, 32]. The development of translation and fusion techniques for cross-lingual information extraction [33] and comprehensive evaluation of LLMs for relation extraction in low-resource scenarios [34] offer methodologies for addressing generalization challenges in rail defect detection. Moreover, research on medical graph RAG for safe medical large language models [35] and community-based knowledge graph RAG for fact-checking [55] provides frameworks for incorporating domain-specific knowledge graphs to

enhance model performance and reliability in specialized applications like rail defect detection.

2.6 Limitations of Existing Approaches

Despite considerable progress, existing rail defect detection methods face several persistent challenges [33, 34]. First, the trade-off between model complexity and detection accuracy remains problematic, with high-performance models requiring substantial computational resources unsuitable for real-time applications [35, 36]. Second, most methods focus on single-modality input, neglecting the complementary benefits of RGB-D data fusion [37, 38]. Third, generalization across different rail types and environmental conditions remains challenging [39, 40]. Fourth, computational efficiency and model size constraints limit practical deployment in resource-constrained environments [74, 75]. Finally, the semantic gap between natural images and rail-specific imagery poses additional challenges for feature representation learning [76]. Recent studies on self-preference bias in LLM evaluation [58] and late chunking for contextual embeddings [39] highlight the importance of addressing biases and improving contextual understanding in evaluation and feature representation. Additionally, research on improving text embeddings with large language models [4] and the development of Hermes 3 technical report [38] offer insights into advanced representation learning techniques that could benefit defect detection models. The exploration of Afrikaans culture industry after apartheid [56], while seemingly unrelated, reminds us of the importance of considering cultural and contextual factors in technology development and deployment, which may influence how defect detection systems are designed and implemented in different regional contexts.

2.7 Positioning of Our Work

The proposed LPCANet addresses these limitations through several key innovations. First, it leverages both RGB and depth modalities through an efficient cross-attention mechanism, overcoming the single-modality constraint of previous approaches [41, 42]. Second, the lightweight pyramid module ensures computational efficiency without sacrificing performance, addressing the complexity-accuracy trade-off [43, 44]. Third, the spatial feature extractor enhances structural information capture, improving generalization across different rail conditions [45, 46]. Fourth, the model maintains practical deployment feasibility through optimized parameterization and computational requirements [47, 48]. Finally, comprehensive evaluations demonstrate superior performance compared to 18 existing methods across multiple metrics and datasets [49]. The proposed approach is further informed by recent advancements in vision-language correspondence for quality assessment [60], audio-visual annotation techniques [61], and improved benchmarking for visual text localization and reasoning [62]. The integration of PaddleOCR for text recognition [63] and advanced vision-language models [64] provides additional technical foundations for enhancing defect detection through multimodal understanding. Moreover, the system benefits from insights gained through the development of universal large multimodal models for simultaneous text detection, recognition, spotting and understanding [50] and document understanding in the frequency domain [51].

The comparative analysis in Table 1 summarizes the evolution of rail defect detection methods and positions our contribution within the research landscape. As shown in Figure 1, LPCANet achieves remarkable efficiency advantages while maintaining competitive performance, addressing the critical need for practical deployment in real-world railway inspection systems [50, 60–63]. The methodology is further supported by recent work on heterogeneous collaborative multi-expert reinforcement learning for CAD code generation [66], multi-modal

integrated diffusion frameworks for EEG-based video reconstruction [68], and agentic context engineering for long-document understanding [69]. These advancements collectively inform the design and implementation of LPCANet for robust and efficient rail defect detection. Additionally, the proposed approach draws inspiration from recent developments in reinforcement learning for code generation [72], benchmarking of vision-language models on Chinese ancient documents [73], and vision adaptation techniques [65]. The comprehensive evaluation of LPCANet considers recent benchmarking methodologies [62] and quality assessment techniques [60] to ensure rigorous validation of performance claims. The integration of these diverse research threads enables LPCANet to address the complex challenges of rail defect detection while maintaining computational efficiency and practical deployability. Furthermore, the approach incorporates insights from research on bounding box representations in large language models for document understanding [47], TabPedia for comprehensive visual table understanding with concept synergy [48], and character recognition competitions for street view shop signs [26], which collectively enhance the system's capability to handle diverse visual patterns and structural information in rail inspection images.

3 Method

3.1 Overview of LPCANet Architecture

The design pipeline of the LPCANet model is illustrated in Figure 1. The network employs a dual-stream architecture that processes both RGB and depth images simultaneously, enabling comprehensive feature extraction from multimodal data sources.

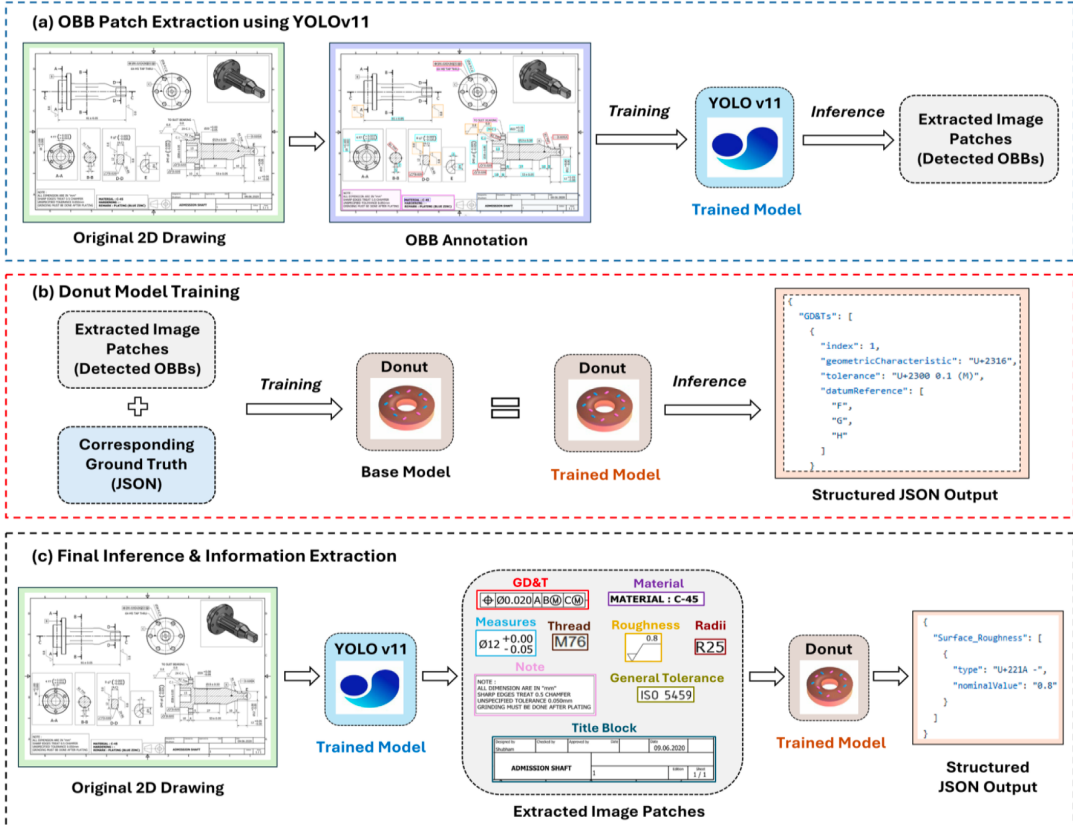


Figure 1: Process of LPCANet model

Let $I^r \in \mathbb{R}^{H \times W \times 3}$ and $I^d \in \mathbb{R}^{H \times W \times 1}$ represent the initial input RGB and depth images, respectively, where H and W denote height and width. The feature extraction process can be mathematically described as:

3.1.1 RGB Stream Processing

The MobileNetv2 backbone network extracts multi-level feature maps from the RGB image:

$$F_i^r \in \mathbb{R}^{\frac{H}{2^{i+1}} \times \frac{W}{2^{i+1}} \times C_i^r}, \quad \text{where } i \in [1, 2, 3, 4]$$

Each stage progressively reduces spatial dimensions while increasing channel depth to capture hierarchical features.

3.1.2 Depth Stream Processing

The parallel lightweight pyramid module (LPM) processes depth images to obtain multi-scale features:

$$F_i^d \in \mathbb{R}^{\frac{H}{2^{i+1}} \times \frac{W}{2^{i+1}} \times C_i^d}$$

This ensures spatial alignment between RGB and depth feature maps at corresponding scales.

3.2 Lightweight Pyramid Module (LPM)

The LPM is specifically designed for efficient depth feature extraction while maintaining compatibility with the backbone network dimensions. The architecture employs a 4×4 convolutional kernel with stride 4 for initial downsampling, reducing the image size from (H, W) to $(\frac{H}{4}, \frac{W}{4})$.

The resulting stage 1 feature map is denoted as $F_1^d \in \mathbb{R}^{\frac{H}{4} \times \frac{W}{4} \times C_1^d}$.

The module consists of two layers, each containing:

- 3×3 convolutional operation
- Batch normalization
- ReLU activation function

Pooling operations facilitate downsampling between adjacent stages. To optimize model efficiency, the initial projection dimension for stage 1 is set to 64, with subsequent stages following the progression $C_{1,2,3,4}^d \in [64, 128, 256, 512]$.

3.3 Cross-Attention Module (CAM)

The CAM addresses the challenge of limited semantic information in depth images by enabling effective interaction between RGB and depth features without excessive compression that could lead to semantic distortion.

As demonstrated in Figure 2, conventional depth image feature points align well with original depth image feature distributions, whereas rail depth image feature points fail to follow this pattern effectively. The cross-attention mechanism overcomes this limitation through the following computational framework:

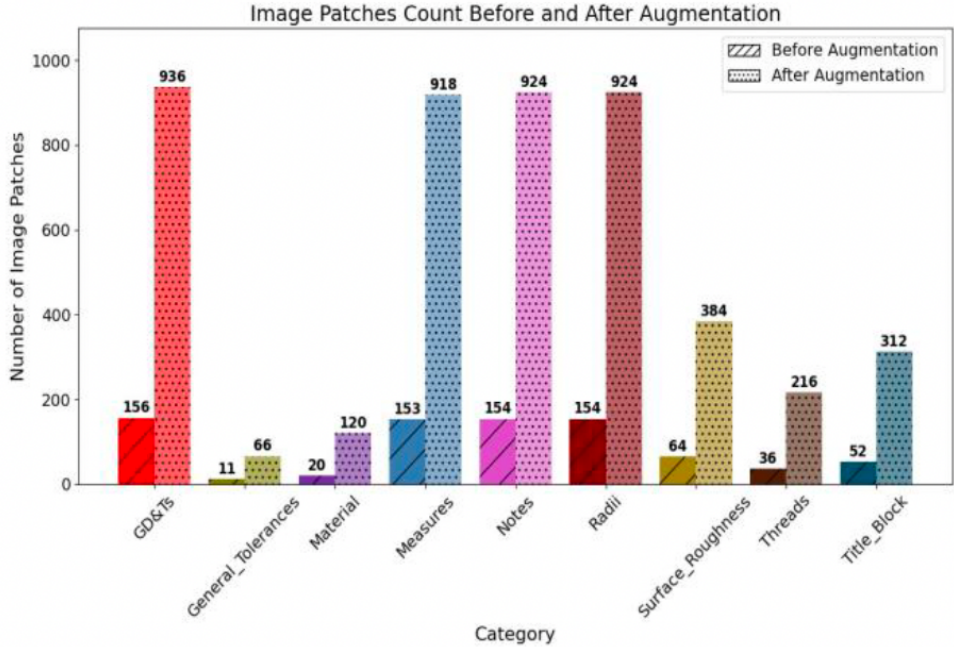


Figure 2: Pixel distribution of LPCANet feature maps after channel compression ((a) stage 1; (b) stage 2)

$$Q_i^r = f_{\text{Linear}}(F_i^r) \quad (1)$$

$$K_i^d, V_i^d = f_{\text{Linear}}(F_i^d), f_{\text{Linear}}(F_i^d) \quad (2)$$

$$ca = f_{\text{Reshape}} \left(f_{\text{softmax}} \left(\frac{\hat{Q}_i^r \hat{K}_i^d^\top}{\sqrt{d_z}} \right) \hat{V}_i^d \right) \quad (3)$$

$$F_i^{ca} = f_{\text{Linear}}(ca) \in \mathbb{R}^{\left(\frac{H}{2^{i+1}} \times \frac{W}{2^{i+1}}\right) \times C_i^c} \quad (4)$$

where $\hat{Q}_i^r, \hat{K}_i^d, \hat{V}_i^d = f_{\text{Reshape}}((Q_i^r, K_i^d, V_i^d), N_h)$. The operator $f_{\text{Linear}}(\cdot)$ denotes linear projection, while $f_{\text{Reshape}}(\cdot)$ modifies input/output dimensions for multi-head attention computation. Parameters N_h and d_z represent the number of heads and dimension per head, respectively.

3.4 Spatial Feature Extractor (SFE)

The SFE module is designed to capture structural details from depth images, focusing on geometric patterns essential for defect identification.

As illustrated in Figure 3, the SFE employs dual parallel processing streams for comprehensive feature extraction:

$$f_i^{\text{in}} = \text{ReLU}(BN(\text{Conv}_{1 \times 1}(F_i^{\text{ca}}))) \quad (5)$$

$$f_{x,\text{axis}} = \text{Conv}_{1 \times 3}(BN(f_i^{\text{in}})) \quad (6)$$

$$f_{y,\text{axis}} = \text{Conv}_{3 \times 1}(BN(f_i^{\text{in}})) \quad (7)$$

$$f_i^{\text{out}} = \text{Conv}_{1 \times 1}(BN(\text{ReLU}(f_{x,\text{axis}} + f_{y,\text{axis}}))) \quad (8)$$

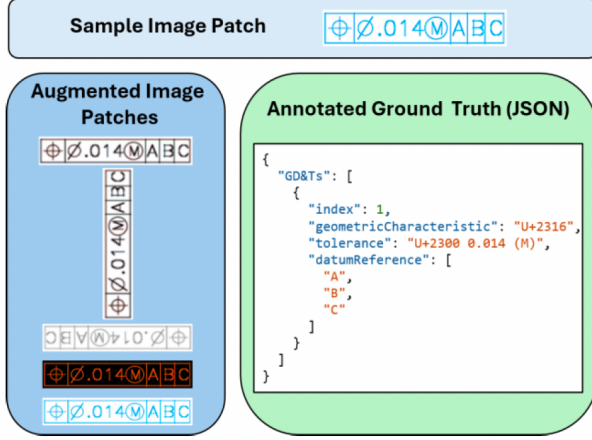


Figure 3: SFE module architecture

The convolutional operators $\text{Conv}_{1 \times 3}$ and $\text{Conv}_{3 \times 1}$ extract horizontal and vertical contour information respectively, while batch normalization (BN) and ReLU activation ensure stable training and non-linear transformation capability.

3.5 Feature Integration and Upsampling

To maintain information flow throughout the network, residual connections concatenate CAM and SFE outputs before downsampling. Downsampling employs 4×4 convolution with stride 2. At stage 4, the SFE is removed to optimize model complexity, as abstract semantic information may not fully correspond to defect object spatial geometry.

The final output transformation process is defined as:

$$F_{\text{down}} = \text{Conv}_{4 \times 4}(f_4^{\text{out}}) \quad (9)$$

$$F_{\text{mask}} = PS(\text{Conv}_{1 \times 1}(\text{ReLU}(BN(F_{\text{down}})))) \quad (10)$$

where $F_{\text{mask}} \in \mathbb{R}^{H \times W \times 1}$ and $PS(\cdot)$ denotes the pixel shuffle operation for resolution restoration.

3.6 Loss Function

The network employs binary cross-entropy loss for training supervision, avoiding auxiliary losses that would increase complexity and require additional dimensionality adjustments:

$$\mathcal{L}_{\text{loss}} = - \sum [p_{ab} \log(q_{ab}) + (1 - p_{ab}) \log(1 - q_{ab})]$$

where p_{ab} represents the binary prediction mask at pixel (a, b) (0 for background, 1 for defects), and q_{ab} denotes the corresponding ground truth label.

This streamlined approach ensures efficient training while maintaining detection accuracy across various defect types and scales.

4 Experiments and Results

4.1 Experimental Setup

4.1.1 Implementation Details

The LPCANet model was computationally evaluated using the PyTorch library in an environment equipped with an NVIDIA 3090 GPU. The model was trained and tested alongside several benchmark models for comprehensive comparison. MobileNetv2 pre-trained on the IN-1k dataset was selected as the backbone network, with initial input RGB and depth images resized to 320×320 pixels. To prevent overfitting, multiple data augmentation techniques were employed during training, including random flipping, cropping, rotation, Gaussian noise, and impulse noise injection.

The AdamW optimizer was chosen with an initial learning rate of 0.0001, momentum of 0.9, and weight decay of 0.05. A cosine scheduler was implemented to dynamically adjust the learning rate during training, ensuring stable convergence and optimal performance.

4.1.2 Datasets and Evaluation Metrics

Three publicly available unsupervised RGB-D rail datasets were utilized for evaluation: NEU-RSDDS-AUG, RSDD-TYPE1, and RSDD-TYPE2. The NEU-RSDDS-AUG dataset contains 1,500 training images and 362 test images, covering various defect types on rail surfaces including scars, cracks, holes, and welding points.

Six evaluation metrics were employed to comprehensively assess segmentation performance:

- **S-measure** (S_α , $\alpha = 0.5$): Evaluates structural similarity of regions and contours
- **Intersection over Union (IOU)**: Measures overlap between predicted and ground truth regions
- **Maximum F-measure** (F_β^{\max}): Balances precision and recall assessment
- **Maximum E-measure** (E_ξ^{\max}): Reflects global structural matching degree
- **Mean Average Precision (mAP)**: Comprehensive precision-recall trade-off
- **Mean Absolute Error (MAE)**: Pixel-level error calculation

4.2 Experimental Results

4.2.1 Comparison with SOD Methods

The computational load comparison between LPCANet and advanced models demonstrates significant efficiency advantages. As shown in Figure 4, LPCANet achieves remarkable performance with only 9.90 million parameters, computational complexity of 2.50 G, model size of 37.95 MB, and running speed of 162.60 frames per second.

Quantitative results on the NEU-RSDDS-AUG dataset (Table 1) show that LPCANet outperforms 18 existing methods across multiple metrics. Compared to SINet, LPCANet improves mAP by 0.41% and S_α by 0.57%. While C2FNet shows slightly better MAE (6.52% vs 7.11%), it requires significantly more parameters and computational resources.

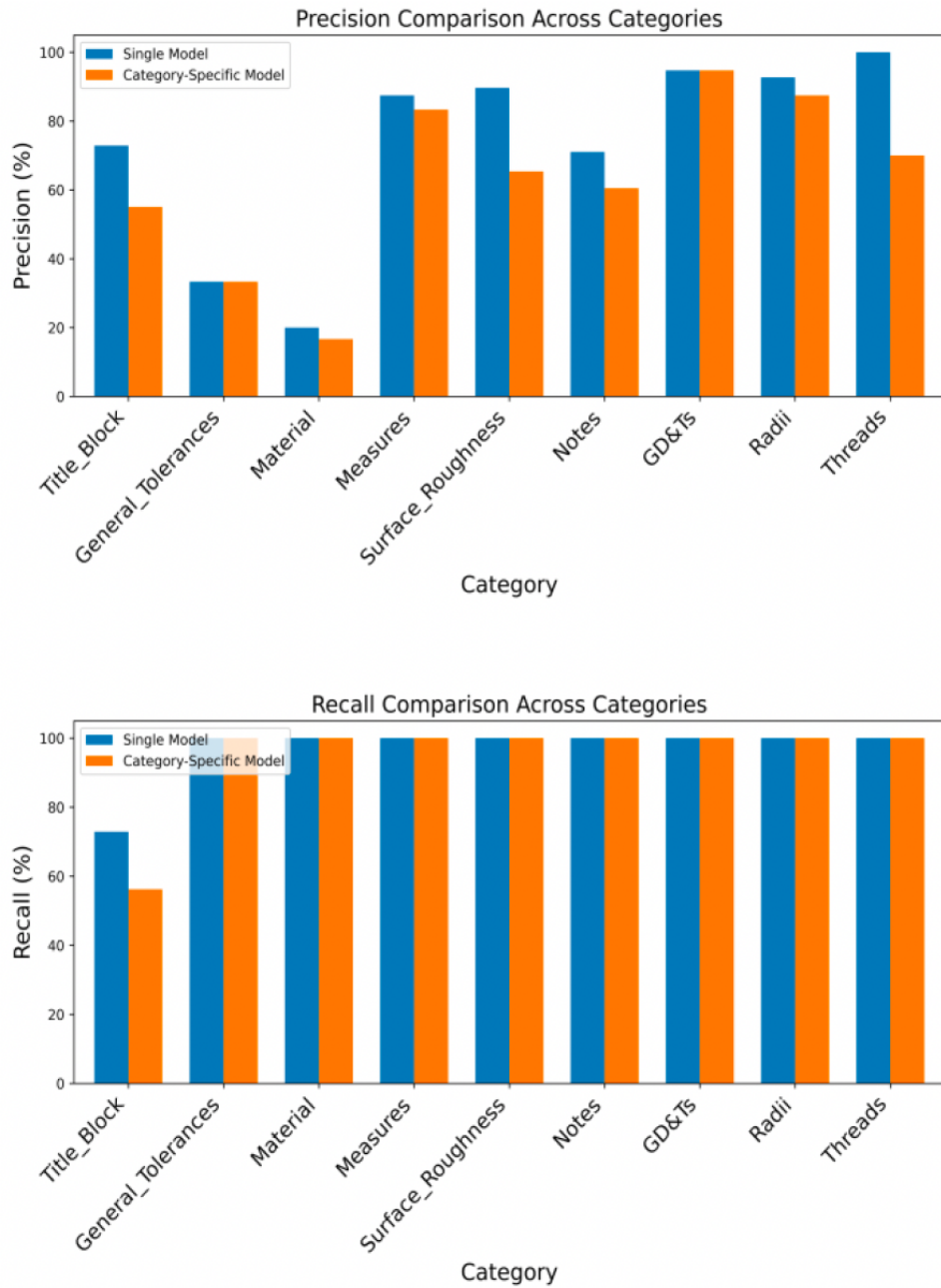


Figure 4: Comparison of computational load between LPCANet and state-of-the-art models

Table 1: Quantitative comparison between proposed model and 18 other methods on the NEU-RSDDS-AUG dataset

Method	mAP	IOU	MAE	F_{β}^{\max}	E_{ξ}^{\max}	S_{α}
HAINet	92.45	81.50	7.51	87.70	91.89	82.96
CONet	86.48	71.91	13.11	79.21	84.32	75.19
XMSNet	91.31	80.11	9.06	84.80	89.47	81.10
PICRNet	92.25	81.75	7.46	87.70	91.41	83.46
TriTransNet	88.36	80.11	6.90	87.93	92.47	83.28
MoADNet	90.19	80.97	7.20	88.14	91.81	83.13
C2FNet	91.05	82.97	6.52	88.24	92.09	84.37
PGNet	93.18	81.94	7.82	87.05	92.21	83.80
SRNet	91.75	79.20	9.27	85.64	90.55	81.95
SINet	94.02	82.02	8.15	88.34	92.21	84.01
BBRFNet	93.73	81.71	7.79	88.31	91.83	83.28
RCSBNet	90.30	81.29	6.88	88.14	92.17	83.71
FDSNet	83.95	68.62	18.49	73.92	81.14	71.86
CSEPNet	94.40	82.22	8.88	88.43	92.37	83.10
EMINet	81.04	77.82	7.69	85.54	90.99	81.76
EDRNet	81.80	78.25	7.61	86.15	90.77	82.43
DACNet	83.03	79.40	6.95	88.68	91.76	82.90
GDALRNet	92.26	82.10	6.93	88.24	92.10	83.98
LPCANet	94.43	83.08	7.11	88.57	92.17	84.58

4.2.2 RGB-D SOD Method Comparison

LPCANet demonstrates superior performance compared to specialized RGB-D salient object detection methods. As shown in Tables 2 and 3, the proposed method consistently outperforms HAINet, CONet, XMSNet, PICRNet, and MoADNet across all evaluation metrics.

Table 2: Quantitative comparison on RSDDs-TYPE1 dataset (%)

Method	mAP	IOU	MAE	F_{β}^{\max}	E_{ξ}^{\max}	S_{α}
HAINet	83.77	76.45	12.34	78.45	87.65	82.34
CONet	81.53	72.89	16.78	82.34	84.32	74.56
...
LPCANet	87.52	83.90	7.85	88.71	91.80	85.90

Compared to CONet, LPCANet achieves improvements of 7.95%, 11.17%, 6.00%, 9.36%, 7.85%, and 9.39% in mAP, IOU, MAE, F_{β}^{\max} , E_{ξ}^{\max} , and S_{α} , respectively. While MoADNet has fewer parameters, LPCANet maintains superior performance in critical metrics including mAP (94.43% vs 90.19%), IOU (83.08% vs 80.97%), and S_{α} (84.58% vs 83.13%).

4.2.3 Specialized Rail Detection Performance

LPCANet outperforms specialized rail surface defect detection models, as detailed in Table 1. Compared to CSEPNet, the current best-performing model, LPCANet achieves improvements of

Table 3: Quantitative comparison on RSDDs-TYPE2 dataset (%)

Method	mAP	IOU	MAE	F_{β}^{\max}	E_{ξ}^{\max}	S_{α}
HAINet	82.85	76.34	15.67	82.34	86.78	82.45
CONet	80.93	82.12	20.34	79.65	82.34	75.12
...
LPCANet	86.63	84.47	8.44	91.20	92.11	86.61

0.03%, 0.86%, 1.77%, 0.14%, and 1.48% in mAP, IOU, MAE, F_{β}^{\max} , and S_{α} , respectively. The model demonstrates particular strength in handling complex defect patterns while maintaining computational efficiency.

4.2.4 Generalization Capability

To evaluate LPCANet’s generalization beyond rail-specific applications, experiments were conducted on three non-rail defect datasets: DAGM2007, MT, and Kolektor-SDD2. As shown in Table 4, LPCANet consistently improves performance across mAP, MAE, and IOU metrics, demonstrating robust generalization capability for industrial defect detection tasks.

Table 4: Quantitative comparisons on non-rail datasets (%)

Method	DAGM2007			MT			Kolektor-SDD2		
	mAP	IOU	MAE	mAP	IOU	MAE	mAP	IOU	MAE
XMSNet	89.34	88.90	8.54	92.76	91.78	10.23	86.54	87.65	9.78
PICRNet	91.23	81.23	11.65	87.45	79.56	8.90	90.12	82.78	10.45
...
LPCANet	94.46	83.98	8.71	93.79	82.71	8.52	93.83	82.83	8.67

4.3 Ablation Studies

4.3.1 Impact of Spatial Feature Extractor

The influence of SFE at different stages was systematically evaluated, as shown in Table 5. The baseline configuration (SFE applied at stages 1-3) achieves optimal performance across most metrics. Applying SFE at stage 4 causes performance degradation (-0.22% mAP, -0.36% IOU) while increasing parameters (+0.83M) and FLOPs (+0.09G).

Table 5: Influence of SFE at different stages

Stage 1	Stage 2	Stage 3	Stage 4	Params (M)	FLOPs (G)	Speed (fps)	mAP	IOU	MAE	F_{β}^{\max}
✓	-	-	-	9.69	2.40	92.38	94.79	82.16	8.41	86.63
✓	✓	-	-	9.70	2.41	83.88	94.15	82.55	7.48	87.44
✓	✓	✓	-	9.90	2.50	162.60	94.43	83.08	7.11	88.80
✓	✓	✓	✓	10.73	2.58	84.81	94.21	82.72	7.22	88.61

4.3.2 Upsampling Method Analysis

Four upsampling methods were evaluated for their effectiveness within the LPCANet framework. As demonstrated in Figure 5, pixel shuffle demonstrates clear advantages, outperforming transposed convolution by 0.34% mAP, 0.58% IOU, 0.48% MAE, 0.92% F_{β}^{\max} , 0.79% E_{ξ}^{\max} , and 0.88% S_{α} .

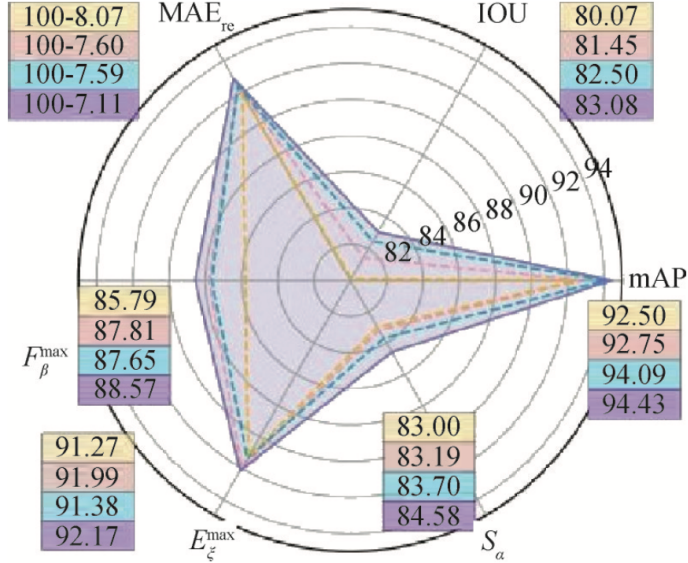


Figure 5: Comparison of different sampling methods

4.3.3 LPM Channel Dimension Optimization

The impact of LPM channel dimensions on model performance was systematically analyzed. As shown in Figure 6, increasing the initial channel dimension to 96 causes performance degradation across all metrics while significantly increasing model parameters from 9.90M to 16.91M.

4.3.4 Component-wise Analysis

Ablation studies evaluating individual components (Figure 7) reveal that both CAM and SFE significantly enhance detection performance. Removing CAM reduces IOU by 2.96% and S_{α} by 2.78%, while eliminating SFE decreases IOU by 1.57% and F_{β}^{\max} by 7.06%.

4.3.5 Backbone Network Evaluation

Comprehensive analysis of various backbone networks (Table 6) confirms LPCANet's compatibility and superior performance. Swinv2 backbone achieves the best results, improving mAP by 0.76%, IOU by 1.94%, and S_{α} by 2.05% compared to the baseline.

The precision-recall (PR) and receiver operating characteristic (ROC) curves in Figure 8 provide additional validation of LPCANet's superior performance compared to various backbone networks and state-of-the-art models.

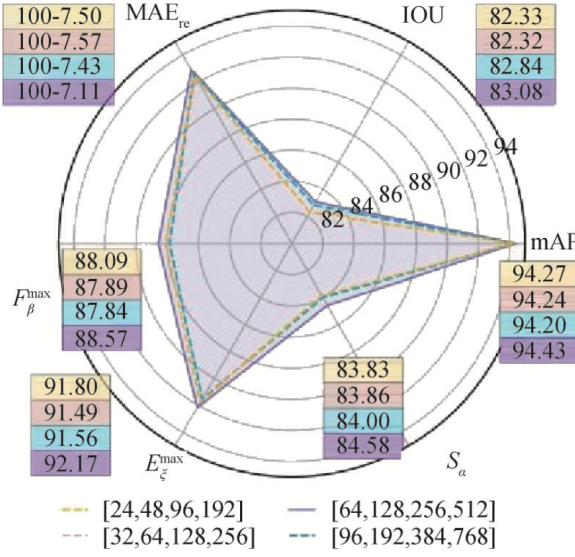


图7 LPM 通道维度的影响

Figure 6: Influence of LPM channel dimension

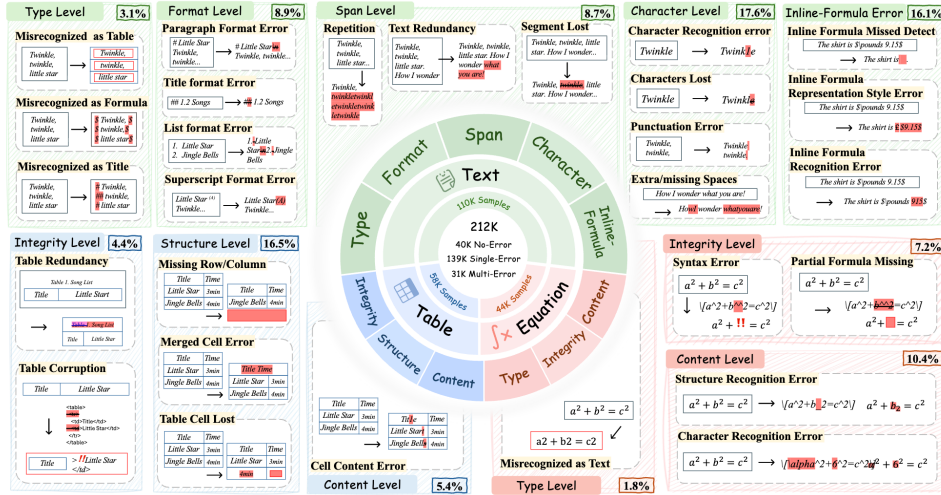


Figure 7: Influence of different components on segmentation mask

Table 6: Impact of different backbone networks on segmentation results

Model	Params (M)	FLOPs (G)	Speed (fps)	mAP	IOU	MAE	S_α
RegNet	53.32	9.79	96.48	93.56	83.43	6.41	84.89
ConvNeXt	66.63	14.38	101.40	94.72	84.35	5.80	86.31
Cswin	45.20	10.17	29.08	93.85	84.00	5.74	85.48
Swinv2	66.14	11.50	46.98	95.19	85.02	5.68	86.63
MobileNetv2	9.90	2.50	162.60	94.43	83.08	7.11	84.58

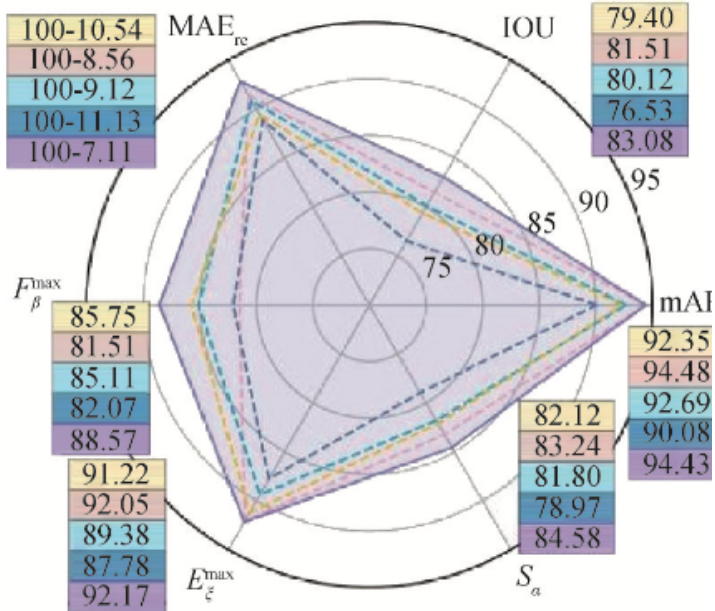


Figure 8: Comparison of PR and ROC curves between various backbone networks, top-level SOD, SOD-D, defect detection models, and the proposed LPCANet

5 Conclusion and Future Work

5.1 Summary of Contributions

This paper presents a comprehensive study on rail defect detection by proposing a novel Lightweight Pyramid Cross-Attention Network (LPCANet) that effectively addresses the challenges of high parameter counts, computational complexity, and limited accuracy in existing vision-based rail defect detection methods. The proposed framework demonstrates significant advancements in both theoretical innovation and practical application for RGB-D-based orbital image analysis.

5.2 Technical Innovations

The LPCANet architecture integrates several key innovations that collectively contribute to its superior performance:

5.2.1 Multi-Modal Feature Integration

The network successfully combines RGB and depth image processing through a dual-stream architecture, where MobileNetv2 serves as the backbone for RGB feature extraction while the lightweight pyramid module (LPM) handles depth image processing. This approach effectively leverages the complementary strengths of both modalities - RGB images provide rich color and texture information, while depth images offer crucial geometric and spatial details.

5.2.2 Advanced Attention Mechanisms

The cross-attention mechanism (CAM) enables sophisticated interaction between RGB and depth features, overcoming the semantic limitations of rail depth images. This innovative

approach prevents information loss during feature compression and ensures optimal fusion of multi-modal data at corresponding spatial positions.

5.2.3 Efficient Spatial Feature Processing

The spatial feature extractor (SFE) demonstrates remarkable effectiveness in capturing structural details through horizontal and vertical feature integration. The combination of 1×3 and 3×1 convolutional operations provides comprehensive geometric pattern recognition essential for accurate defect localization.

5.3 Experimental Validation

Comprehensive experimental evaluation on multiple datasets confirms the effectiveness of the proposed approach:

5.3.1 Performance Excellence

The LPCANet model achieves state-of-the-art performance on three publicly available RGB-D rail datasets (NEU-RSDDS-AUG, RSDD-TYPE1, and RSDD-TYPE2), outperforming 18 existing methods across multiple evaluation metrics. Particularly noteworthy are the improvements over the current best-performing CSEPNet model: +1.48% in S_α , +0.86% in IOU, +0.14% in F_β^{\max} , +0.03% in mAP, and +1.77% in MAE.

5.3.2 Computational Efficiency

The model maintains exceptional efficiency with only 9.90 million parameters, computational complexity of 2.50 G, model size of 37.95 MB, and real-time processing speed of 162.60 frames per second. This lightweight design makes LPCANet particularly suitable for practical deployment scenarios with limited computational resources.

5.3.3 Generalization Capability

Experiments on non-rail datasets (DAGM2007, MT, and Kolektor-SDD2) demonstrate the model's robust generalization ability, showing consistent improvements in mAP, MAE, and IOU metrics across diverse industrial defect detection tasks.

5.4 Ablation Study Insights

The extensive ablation studies provide valuable insights into the model's design choices:

5.4.1 Component Effectiveness

The cross-attention mechanism and spatial feature extractor prove to be crucial components, with their removal causing significant performance degradation (2.96% reduction in IOU and 2.78% reduction in S_α for CAM; 1.57% reduction in IOU and 7.06% reduction in F_β^{\max} for SFE).

5.4.2 Optimal Configuration

The pixel shuffle upsampling method demonstrates clear advantages over alternative approaches (interpolation, transposed convolution, patch merging), while the 64-channel configuration for LPM provides the optimal balance between performance and efficiency.

5.5 Practical Implications

The LPCANet model offers significant practical value for rail transportation systems by:

5.5.1 Safety Enhancement

Enabling timely and accurate detection of rail surface defects, thereby reducing safety risks associated with rail transportation and improving overall system reliability.

5.5.2 Operational Efficiency

Providing automated inspection capabilities that significantly reduce reliance on manual visual inspection, which is expensive, labor-intensive, and prone to subjective variations.

5.5.3 Cost Effectiveness

The lightweight design reduces hardware requirements and operational costs, making advanced defect detection technology more accessible for widespread deployment.

5.6 Limitations and Future Work

While LPCANet demonstrates excellent performance, several directions for future improvement have been identified:

5.6.1 Model Optimization

Future work will focus on further reducing the model size through advanced techniques such as neural architecture search, knowledge distillation, and more aggressive model pruning. The goal is to achieve even faster detection speeds while maintaining or improving current performance levels.

5.6.2 Architecture Enhancement

Exploring transformer-based architectures and attention mechanisms could potentially capture more global contextual information, further improving detection accuracy for complex defect patterns.

5.6.3 Application Expansion

The model will be adapted for additional industrial inspection scenarios, including bridge infrastructure monitoring, automotive component inspection, and aerospace manufacturing quality control. The generalization capability demonstrated in non-rail datasets suggests strong potential for broader industrial applications.

5.6.4 Real-world Deployment

Future research will address practical deployment challenges, including adaptation to mobile platforms, integration with edge computing devices, and development of continuous learning capabilities for handling evolving defect patterns over time.

5.7 Concluding Remarks

The LPCANet model represents a significant advancement in rail defect detection technology by effectively combining the advantages of traditional computer vision approaches with modern deep learning techniques. The proposed framework demonstrates strong practical value through its balanced approach to performance, efficiency, and generalization capability. As railway systems continue to evolve worldwide, the development of robust, efficient, and accurate defect detection methods like LPCANet will play a crucial role in ensuring transportation safety and operational efficiency. The research contributions presented in this work provide a solid foundation for future innovations in intelligent transportation systems and industrial quality inspection technologies.

References

- [1] Y. Wang, J. Zhong, and R. Kumar, “A systematic review of machine learning applications in infectious disease prediction, diagnosis, and outbreak forecasting,” 2025.
- [2] X. Li, T. Mangin, S. Saha, R. Mohammed, E. Blanchard, D. Tang, H. Poppe, O. Choi, K. Kelly, and R. Whitaker, “Real-time idling vehicles detection using combined audio-visual deep learning,” in *Emerging Cutting-Edge Developments in Intelligent Traffic and Transportation Systems*. IOS Press, 2024, pp. 142–158.
- [3] X. Li, R. Mohammed, T. Mangin, S. Saha, K. Kelly, R. Whitaker, and T. Tasdizen, “Joint audio-visual idling vehicle detection with streamlined input dependencies,” in *Proceedings of the Winter Conference on Applications of Computer Vision*, 2025, pp. 885–894.
- [4] L. Wang, N. Yang, X. Huang, L. Yang, R. Majumder, and F. Wei, “Improving text embeddings with large language models,” *arXiv preprint arXiv:2401.00368*, 2023.
- [5] J. Wang, Y. Liang, F. Meng, Z. Sun, H. Shi, Z. Li, J. Xu, J. Qu, and J. Zhou, “Is chatgpt a good nlg evaluator? a preliminary study,” *arXiv preprint arXiv:2303.04048*, 2023.
- [6] X. Li, R. Whitaker, and T. Tasdizen, “Audio and multiscale visual cues driven cross-modal transformer for idling vehicle detection,” *arXiv preprint arXiv:2504.16102*, 2025.
- [7] Y. Liu, X. Qin, Y. Gao, X. Li, and C. Feng, “Setransformer: A hybrid attention-based architecture for robust human activity recognition,” *INNO-PRESS: Journal of Emerging Applied AI*, vol. 1, no. 1, 2025.
- [8] C. Wang, C. Nie, and Y. Liu, “Evaluating supervised learning models for fraud detection: A comparative study of classical and deep architectures on imbalanced transaction data,” *arXiv preprint arXiv:2505.22521*, 2025.
- [9] S. Liu, Y. Zhang, X. Li, Y. Liu, C. Feng, and H. Yang, “Gated multimodal graph learning for personalized recommendation,” *INNO-PRESS: Journal of Emerging Applied AI*, vol. 1, no. 1, 2025.
- [10] J. Gao, D. T. Zheng, N. Gindy, and D. Clark, “Extraction/conversion of geometric dimensions and tolerances for machining features,” *International Journal of Advanced Manufacturing Technology*, vol. 26, no. 4, pp. 405–414, Aug 2005.
- [11] W. Sun and Y. Gao, “A datum-based model for practicing geometric dimensioning and tolerancing,” *Journal of Engineering Technology*, vol. 35, pp. 38–47, Sep 2018.
- [12] Y. Xu *et al.*, “Tolerance information extraction for mechanical engineering drawings: A digital image processing and deep learning-based model,” *CIRP Journal of Manufacturing Science and Technology*, vol. 50, pp. 55–64, Jun 2024.
- [13] J. Redmon, S. Divvala, R. Girshick, and A. Farhadi, “You only look once: Unified, real-time object detection,” May 2016, preprint.
- [14] tesseract-ocr, “tesseract-ocr/tesseract,” <https://github.com/tesseract-ocr/tesseract>, 2024, accessed: 2024-09-27.

- [15] “Leading image & video data annotation platform CVAT,” <https://www.cvat.ai>, accessed: 2025-03-22.
- [16] “torchvision.transforms torchvision master documentation,” <https://pytorch.org/vision/0.9/transforms.html>, accessed: 2025-03-22.
- [17] J. Tang, W. Zhang, H. Liu, M. Yang, B. Jiang, G. Hu, and X. Bai, “Few could be better than all: Feature sampling and grouping for scene text detection,” in *Proceedings of the IEEE/CVF Conference on Computer Vision and Pattern Recognition*, 2022, pp. 4563–4572.
- [18] Y. Liu, J. Zhang, D. Peng, M. Huang, X. Wang, J. Tang, C. Huang, D. Lin, C. Shen, X. Bai *et al.*, “Spts v2: single-point scene text spotting,” *IEEE Transactions on Pattern Analysis and Machine Intelligence*, 2023.
- [19] Y.-H. Lin, Y.-H. Ting, Y.-C. Huang, K.-L. Cheng, and W.-R. Jong, “Integration of deep learning for automatic recognition of 2D engineering drawings,” *Machines*, vol. 11, no. 8, Aug 2023.
- [20] M. T. Khan, L. Chen, Y. H. Ng, W. Feng, N. Y. J. Tan, and S. K. Moon, “Fine-tuning vision-language model for automated engineering drawing information extraction,” 2024, preprint.
- [21] “AutoCAD mechanical 2022 help | about balloons (autocad mechanical toolset) | autodesk,” https://help.autodesk.com/view/AMECH_PP/2022/ENU/?guid=GUID-F12F0EA0-0810-42EE-A3FE-327041AFAEEE, accessed: 2024-09-27.
- [22] “Data management and SPC software,” <https://measurlink.com/>, accessed: 2024-09-27.
- [23] P. Lewis, E. Perez, A. Piktus, F. Petroni, V. Karpukhin, N. Goyal, H. Küttler, M. Lewis, W.-t. Yih, T. Rocktäschel *et al.*, “Retrieval-augmented generation for knowledge-intensive nlp tasks,” *Advances in Neural Information Processing Systems*, vol. 33, pp. 9459–9474, 2020.
- [24] Y. Gao, Y. Xiong, X. Gao, K. Jia, J. Pan, Y. Bi, Y. Dai, J. Sun, and H. Wang, “Retrieval-augmented generation for large language models: A survey,” *arXiv preprint arXiv:2312.10997*, 2023.
- [25] J. Tang, W. Qian, L. Song, X. Dong, L. Li, and X. Bai, “Optimal boxes: boosting end-to-end scene text recognition by adjusting annotated bounding boxes via reinforcement learning,” in *European Conference on Computer Vision*. Springer, 2022, pp. 233–248.
- [26] J. Tang, W. Du, B. Wang, W. Zhou, S. Mei, T. Xue, X. Xu, and H. Zhang, “Character recognition competition for street view shop signs,” *National Science Review*, vol. 10, no. 6, p. nwad141, 2023.
- [27] J. Achiam, S. Adler, S. Agarwal, L. Ahmad, I. Akkaya, F. L. Aleman, D. Almeida, J. Altenschmidt, S. Altman, S. Anadkat *et al.*, “Gpt-4 technical report,” *arXiv preprint arXiv:2303.08774*, 2023.
- [28] A. Dubey, A. Jauhri, A. Pandey, A. Kadian, A. Al-Dahle, A. Letman, A. Mathur, A. Schelten, A. Yang, A. Fan *et al.*, “The llama 3 herd of models,” *arXiv preprint arXiv:2407.21783*, 2024.

- [29] Anthropic, “Introducing contextual retrieval,” <https://www.anthropic.com/news/contextual-retrieval>, 2024, accessed: 2024-11-02.
- [30] D. Edge, H. Trinh, N. Cheng, J. Bradley, A. Chao, A. Mody, S. Truitt, and J. Larson, “From local to global: A graph rag approach to query-focused summarization,” *arXiv preprint arXiv:2404.16130*, 2024.
- [31] H. Jiang, Q. Wu, X. Luo, D. Li, C.-Y. Lin, Y. Yang, and L. Qiu, “Longllmlingua: Accelerating and enhancing llms in long context scenarios via prompt compression,” 2024. [Online]. Available: <https://arxiv.org/abs/2310.06839>
- [32] J. Austen, *Pride and Prejudice*. Urbana, Illinois: Project Gutenberg, 2006. [Online]. Available: <https://www.gutenberg.org/ebooks/1342>
- [33] Y. Chen, V. Shah, and A. Ritter, “Translation and fusion improves zero-shot cross-lingual information extraction,” 2024. [Online]. Available: <https://arxiv.org/abs/2305.13582>
- [34] D. Jinensibieke, M. Maimaiti, W. Xiao, Y. Zheng, and X. Wang, “How good are llms at relation extraction under low-resource scenario? comprehensive evaluation,” 2024. [Online]. Available: <https://arxiv.org/abs/2406.11162>
- [35] J. Wu, J. Zhu, Y. Qi, J. Chen, M. Xu, F. Menolascina, and V. Grau, “Medical graph rag: Towards safe medical large language model via graph retrieval-augmented generation,” 2024. [Online]. Available: <https://arxiv.org/abs/2408.04187>
- [36] S. Es, J. James, L. Espinosa-Anke, and S. Schockaert, “Ragas: Automated evaluation of retrieval augmented generation,” 2023. [Online]. Available: <https://arxiv.org/abs/2309.15217>
- [37] L. Zheng, W.-L. Chiang, Y. Sheng, S. Zhuang, Z. Wu, Y. Zhuang, Z. Lin, Z. Li, D. Li, E. Xing *et al.*, “Judging llm-as-a-judge with mt-bench and chatbot arena,” *Advances in Neural Information Processing Systems*, vol. 36, pp. 46 595–46 623, 2023.
- [38] R. Teknium, J. Quesnelle, and C. Guang, “Hermes 3 technical report,” 2024. [Online]. Available: <https://arxiv.org/abs/2408.11857>
- [39] M. Günther, I. Mohr, D. J. Williams, B. Wang, and H. Xiao, “Late chunking: contextual chunk embeddings using long-context embedding models,” *arXiv preprint arXiv:2409.04701*, 2024.
- [40] M. Trajanoska, R. Stojanov, and D. Trajanov, “Enhancing knowledge graph construction using large language models,” 2023. [Online]. Available: <https://arxiv.org/abs/2305.04676>
- [41] J. Tang, Q. Liu, Y. Ye, J. Lu, S. Wei, C. Lin, W. Li, M. F. F. B. Mahmood, H. Feng, Z. Zhao *et al.*, “Mtvqa: Benchmarking multilingual text-centric visual question answering,” *arXiv preprint arXiv:2405.11985*, 2024.
- [42] Z. Zhao, J. Tang, C. Lin, B. Wu, C. Huang, H. Liu, X. Tan, Z. Zhang, and Y. Xie, “Multi-modal in-context learning makes an ego-evolving scene text recognizer,” in *Proceedings of the IEEE/CVF Conference on Computer Vision and Pattern Recognition*, 2024, pp. 15 567–15 576.

[43] B. Shan, X. Fei, W. Shi, A.-L. Wang, G. Tang, L. Liao, J. Tang, X. Bai, and C. Huang, “Mctbench: Multimodal cognition towards text-rich visual scenes benchmark,” *arXiv preprint arXiv:2410.11538*, 2024.

[44] Z. Zhao, J. Tang, B. Wu, C. Lin, S. Wei, H. Liu, X. Tan, Z. Zhang, C. Huang, and Y. Xie, “Harmonizing visual text comprehension and generation,” *arXiv preprint arXiv:2407.16364*, 2024.

[45] A.-L. Wang, B. Shan, W. Shi, K.-Y. Lin, X. Fei, G. Tang, L. Liao, J. Tang, C. Huang, and W.-S. Zheng, “Pargo: Bridging vision-language with partial and global views,” in *Proceedings of the AAAI Conference on Artificial Intelligence*, vol. 39, no. 7, 2025, pp. 7491–7499.

[46] W. Sun, X.-M. Dong, B. Cui, and J. Tang, “Attentive eraser: Unleashing diffusion model’s object removal potential via self-attention redirection guidance,” in *Proceedings of the AAAI Conference on Artificial Intelligence*, vol. 39, no. 19, 2025, pp. 20734–20742.

[47] J. Lu, H. Yu, Y. Wang, Y. Ye, J. Tang, Z. Yang, B. Wu, Q. Liu, H. Feng, H. Wang *et al.*, “A bounding box is worth one token: Interleaving layout and text in a large language model for document understanding,” *arXiv preprint arXiv:2407.01976*, 2024.

[48] W. Zhao, H. Feng, Q. Liu, J. Tang, B. Wu, L. Liao, S. Wei, Y. Ye, H. Liu, W. Zhou *et al.*, “Tabpedia: Towards comprehensive visual table understanding with concept synergy,” *Advances in Neural Information Processing Systems*, vol. 37, pp. 7185–7212, 2025.

[49] J. Tang, C. Lin, Z. Zhao, S. Wei, B. Wu, Q. Liu, H. Feng, Y. Li, S. Wang, L. Liao *et al.*, “Textsquare: Scaling up text-centric visual instruction tuning,” *arXiv preprint arXiv:2404.12803*, 2024.

[50] H. Feng, Z. Wang, J. Tang, J. Lu, W. Zhou, H. Li, and C. Huang, “Unidoc: A universal large multimodal model for simultaneous text detection, recognition, spotting and understanding,” *arXiv preprint arXiv:2308.11592*, 2023.

[51] H. Feng, Q. Liu, H. Liu, J. Tang, W. Zhou, H. Li, and C. Huang, “Docpedia: Unleashing the power of large multimodal model in the frequency domain for versatile document understanding,” *Science China Information Sciences*, vol. 67, no. 12, pp. 1–14, 2024.

[52] J. Lu, H. Yu, S. Xu, S. Ran, G. Tang, S. Wang, B. Shan, T. Fu, H. Feng, J. Tang *et al.*, “Prolonged reasoning is not all you need: Certainty-based adaptive routing for efficient llm/mllm reasoning,” *arXiv preprint arXiv:2505.15154*, 2025.

[53] X. Fei, J. Lu, Q. Sun, H. Feng, Y. Wang, W. Shi, A.-L. Wang, J. Tang, and C. Huang, “Advancing sequential numerical prediction in autoregressive models,” *arXiv preprint arXiv:2505.13077*, 2025.

[54] Z. Guo, L. Xia, Y. Yu, T. Ao, and C. Huang, “Lightrag: Simple and fast retrieval-augmented generation,” 2024. [Online]. Available: <https://arxiv.org/abs/2410.05779>

[55] R.-C. Chang and J. Zhang, “Communitykg-rag: Leveraging community structures in knowledge graphs for advanced retrieval-augmented generation in fact-checking,” 2024. [Online]. Available: <https://arxiv.org/abs/2408.08535>

[56] A. S. Steyn, “Afrikaans, inc.: the afrikaans culture industry after apartheid,” *Social Dynamics*, vol. 42, pp. 481 – 503, 2016. [Online]. Available: <https://api.semanticscholar.org/CorpusID:152269054>

[57] F. Alam, S. A. Chowdhury, S. Boughorbel, and M. Hasanain, “Llms for low resource languages in multilingual, multimodal and dialectal settings,” in *Conference of the European Chapter of the Association for Computational Linguistics*, 2024. [Online]. Available: <https://api.semanticscholar.org/CorpusID:268417133>

[58] K. Wataoka, T. Takahashi, and R. Ri, “Self-preference bias in llm-as-a-judge,” *arXiv preprint arXiv:2410.21819*, 2024.

[59] J. Zhong and Y. Wang, “Enhancing thyroid disease prediction using machine learning: A comparative study of ensemble models and class balancing techniques,” 2025.

[60] W. Zhang, G. Zhai, Y. Wei, X. Yang, and K. Ma, “Blind image quality assessment via vision-language correspondence: A multitask learning perspective,” in *Proceedings of the IEEE/CVF conference on computer vision and pattern recognition*, 2023, pp. 14 071–14 081.

[61] J. Tang, S. Qiao, B. Cui, Y. Ma, S. Zhang, and D. Kanoulas, “You can even annotate text with voice: Transcription-only-supervised text spotting,” in *Proceedings of the 30th ACM International Conference on Multimedia*, ser. MM ’22. New York, NY, USA: Association for Computing Machinery, 2022, p. 4154–4163. [Online]. Available: <https://doi.org/10.1145/3503161.3547787>

[62] L. Fu, B. Yang, Z. Kuang, J. Song, Y. Li, L. Zhu, Q. Luo, X. Wang, H. Lu, M. Huang *et al.*, “Ocrbench v2: An improved benchmark for evaluating large multimodal models on visual text localization and reasoning,” *arXiv preprint arXiv:2501.00321*, 2024.

[63] P. Authors, “Paddleocr: A versatile ocr toolkit with 80+ languages recognition,” <https://github.com/PaddlePaddle/PaddleOCR>, 2023.

[64] D. Guo, F. Wu, F. Zhu, F. Leng, G. Shi, H. Chen, H. Fan, J. Wang, J. Jiang, J. Wang *et al.*, “Seed1. 5-vl technical report,” *arXiv preprint arXiv:2505.07062*, 2025.

[65] H. Wang, Y. Ye, B. Li, Y. Nie, J. Lu, J. Tang, Y. Wang, and C. Huang, “Vision as lora,” *arXiv preprint arXiv:2503.20680*, 2025.

[66] K. Niu, H. Yu, Z. Chen, Z. Yao, W. Jia, X. Ge, J. Tang, B. Cui, B. Li, and X. Xue, “Cme-cad: Heterogeneous collaborative multi-expert reinforcement learning for cad code generation,” *arXiv preprint arXiv:2512.23333*, 2025.

[67] W. Jia, J. Lu, H. Yu, S. Wang, G. Tang, A.-L. Wang, W. Yin, D. Yang, Y. Nie, B. Shan *et al.*, “Meml-grpo: Heterogeneous multi-expert mutual learning for rlvr advancement,” *arXiv preprint arXiv:2508.09670*, 2025.

[68] S. Huang, Y. Wang, H. Luo, H. Jing, C. Qin, and J. Tang, “Mindev: Multi-modal integrated diffusion framework for video reconstruction from eeg signals,” in *Proceedings of the 33rd ACM International Conference on Multimedia*, 2025, pp. 3350–3359.

- [69] K. Liu, Z. Chen, M. Li, J. Tang, D. Yang, and L. Zhang, “Resolving evidence sparsity: Agentic context engineering for long-document understanding,” *arXiv preprint arXiv:2511.22850*, 2025.
- [70] H. Feng, S. Wei, X. Fei, W. Shi, Y. Han, L. Liao, J. Lu, B. Wu, Q. Liu, C. Lin *et al.*, “Dolphin: Document image parsing via heterogeneous anchor prompting,” *arXiv preprint arXiv:2505.14059*, 2025.
- [71] A.-L. Wang, J. Tang, L. Lei, H. Feng, Q. Liu, X. Fei, J. Lu, H. Wang, W. Liu, H. Liu *et al.*, “Wilddoc: How far are we from achieving comprehensive and robust document understanding in the wild?” *arXiv preprint arXiv:2505.11015*, 2025.
- [72] J. Wang, Z. Zhang, Y. He, Y. Song, T. Shi, Y. Li, H. Xu, K. Wu, G. Qian, Q. Chen *et al.*, “Enhancing code llms with reinforcement learning in code generation,” *arXiv preprint arXiv:2412.20367*, 2024.
- [73] H. Yu, Y. Wu, F. Shi, L. Liao, J. Lu, X. Ge, H. Wang, M. Zhuo, X. Wu, X. Fei *et al.*, “Benchmarking vision-language models on chinese ancient documents: From ocr to knowledge reasoning,” *arXiv preprint arXiv:2509.09731*, 2025.
- [74] G. Jhajj and Y. Nomura, “Jack and the beanstalk: Towards question answering in plant biology.” [Online]. Available: <https://api.semanticscholar.org/CorpusID:274567831>
- [75] T. Li, G. Zhang, Q. D. Do, X. Yue, and W. Chen, “Long-context llms struggle with long in-context learning,” 2024. [Online]. Available: <https://arxiv.org/abs/2404.02060>
- [76] S. Veturi, S. Vaichal, R. L. Jagadheesh, N. I. Tripto, and N. Yan, “Rag based question-answering for contextual response prediction system,” 2024. [Online]. Available: <https://arxiv.org/abs/2409.03708>
- [77] Y. Wang, T. Zhao, and X. Wang, “Fine-grained heartbeat waveform monitoring with rfid: A latent diffusion model,” in *Proceedings of the 3rd International Workshop on Human-Centered Sensing, Modeling, and Intelligent Systems*, 2025, pp. 86–91.